Increased plasmin-mediated proteolysis of L1CAM in a mouse model of idiopathic normal pressure hydrocephalus

Dejun Yang[a,1], Hongwei Yang[a,1], Gabrielle Luiselli[a], Charles Ogagan[a], Huijun Dai[a], Lucinda Chiu[a], Rona S. Carroll[a], and Mark D. Johnson[a,2]

[a]Department of Neurological Surgery, University of Massachusetts Medical School, University of Massachusetts Memorial Healthcare, Worcester, MA 01655

Idiopathic normal pressure hydrocephalus (iNPH) is a common neurological disorder that is characterized by enlarged cerebral ventricles, gait difficulty, incontinence, and dementia. iNPH usually develops after the sixth decade of life in previously asymptomatic individuals. We recently reported that loss-of-function deletions in *CWH43* lead to the development of iNPH in a subgroup of patients, but how this occurs is poorly understood. Here, we show that deletions in *CWH43* decrease expression of the cell adhesion molecule, L1CAM, in the brains of *CWH43* mutant mice and in human HeLa cells harboring a *CWH43* deletion. Loss-of-function mutations in L1CAM are a common cause of severe neurodevelopmental defects that include congenital X-linked hydrocephalus. Mechanistically, we find that *CWH43* deletion leads to decreased N-glycosylation of L1CAM, decreased association of L1CAM with cell membrane lipid microdomains, increased L1CAM cleavage by plasmin, and increased shedding of cleaved L1CAM in the cerebrospinal fluid. *CWH43* deletion also decreased L1CAM nuclear translocation, suggesting decreased L1CAM intracellular signaling. Importantly, the increase in L1CAM cleavage occurred primarily in the ventricular and subventricular zones where brain *CWH43* is most highly expressed. Thus, *CWH43* deletions may contribute to adult-onset iNPH by selectively downregulating L1CAM in the ventricular and subventricular zone.

normal pressure hydrocephalus | L1CAM | CWH43 | plasmin | hydrocephalus

Idiopathic normal pressure hydrocephalus (iNPH) is a neurological disorder that is characterized by enlarged cerebral ventricles, gait difficulty, incontinence, and dementia (1). iNPH usually develops after the sixth decade of life in previously asymptomatic individuals (2). Approximately 1% of individuals over the age of 60 and 5.6% of individuals over 75 y of age develop the disorder (3–6). Until recently, the cause of iNPH was unknown. However, we recently reported that about 15% of patients with sporadic iNPH harbor heterozygous deletions in *CWH43* (7), which encodes a protein that incorporates ceramide into the lipid anchor of glycosylphosphatidylinositol (GPI)–anchored proteins (8). Mice harboring *CWH43* deletions appear behaviorally normal but develop communicating hydrocephalus and gait imbalance. Inspection of the ventricular zone in *CWH43* mutant mice revealed a decrease in the number of ventricular cilia and decreased apical localization of GPI-anchored proteins in choroid plexus and ependymal cells. How these changes relate to the development of hydrocephalus in *CWH43* mutant mice is unclear.

One of the most common causes of X-linked congenital hydrocephalus in humans is mutation of *L1CAM* (9). L1CAM (also known as L1) is a transmembrane glycoprotein that promotes cell adhesion, migration, neurite outgrowth, and myelination through homophilic binding or heterophilic binding to integrins and other proteins (10). In humans, *L1CAM* mutations can cause severe neurodevelopmental defects including corpus callosum agenesis, mental retardation, adducted thumbs, spastic paraplegia, and

hydrocephalus (i.e., L1 syndrome) (9). Mice harboring *L1CAM* mutations also display hydrocephalus and severe neurodevelopmental abnormalities (11).

The L1CAM protein contains six extracellular immunoglobulin domains, five fibronectin type III (FNIII) domains, a transmembrane domain, and an intracellular domain (10). L1CAM activity is controlled at both the transcriptional and posttranscriptional levels. N-glycosylation, fucosylation, sumoylation, phosphorylation, or cleavage of L1CAM all regulate L1CAM binding or signaling (12–15). L1CAM binding can activate intracellular kinase signaling pathways (10, 11), and L1CAM cleavage can release the intracellular domain, which then signals through cytoplasmic and nuclear pathways. The extracellular domain of L1CAM can be cleaved by several different proteases to release soluble extracellular fragments that act as ligands and retain biological activity. ADAM10, ADAM17, BACE1, Reelin, and myelin basic protein cleave L1CAM proximally to shed soluble extracellular L1CAM fragments from the cell surface (16–19). Cleavage by plasmin (20) or proprotein convertase PC5A (21) in the third fibronectin domain also generates a soluble extracellular fragment that stimulates neurite outgrowth and cell adhesion, although studies suggest that this fragment may be less effective in promoting protein multimerization, integrin binding, cell adhesion, and myelination.

Significance

Idiopathic normal pressure hydrocephalus (iNPH) is the most common form of adult-onset hydrocephalus, but its etiology is poorly understood. Symptoms develop in previously normal individuals and include gait difficulty, incontinence, and dementia. We recently reported that 15% of iNPH patients harbor heterozygous loss-of-function deletions in CWH43, which encodes a protein that modifies other cell membrane proteins. Mice harboring CWH43 deletions develop hydrocephalus and gait dysfunction. Mutations affecting the L1CAM adhesion protein cause developmental brain abnormalities and hydrocephalus from birth. Here, we show that CWH43 deletion leads to L1CAM hypoglycosylation, decreased L1CAM association with lipid microdomains, increased plasmin-mediated L1CAM cleavage, and decreased L1CAM expression. Thus, decreased L1CAM expression appears to occur in adult-onset iNPH and congenital hydrocephalus.

NEUROSCIENCE

www.manaraa.com

Indeed, evidence suggests that extracellular L1CAM fragments generated by different proteases may have different biological activity during development.

Here, we show that in human cells in vitro and in the mouse brain, *CWH43* deletion leads to hypoglycosylation of L1CAM, decreased L1CAM association with lipid microdomains, increased L1CAM proteolysis by plasmin, and decreased L1CAM expression primarily in the ventricular region where Cwh43 expression is high. Our findings may help to explain the lack of neurodevelopmental deficits and the late onset of symptoms seen in patients with adult-onset iNPH.

Materials and Methods

Animals. All experiments and procedures involving mice were approved by the University of Massachusetts Medical School Institutional Animal Care and Use Committee. C57bl6 mice harboring a Met533Ter mutation (coinciding to the human *CWH43* deletion 4:49034669 CA/C; Leu533Ter) were generated using a CRISPR/Cas9 approach and bred to generate homozygous (*CWH43^{M533/M533}*) animals as described previously (7). This mutation generates a stop codon that truncates the encoded Cwh43 protein and disrupts its function.

Cell Culture and Compound Treatment. A human HeLa cell line bearing the *CWH43* mutation was generated as described (7). Cells were maintained in Dulbecco's modified Eagle's medium (DMEM) (Invitrogen) supplemented with 10% fetal bovine serum (Invitrogen). For some experiments, HeLa cells were maintained in a serum-free medium. Cells were incubated in the presence of compounds of interest with or without serum for 8–12 h before harvest. Compounds used included recombinant plasmin (20 or 50 μg/mL; P1867; Sigma-Aldrich); α$_2$ antiplasmin (70 μg/mL; 178221; Sigma-Aldrich); an ADAM metallopeptidase domain 10 (ADAM10) inhibitor GI254023X (0.5–2 μg/mL; SML0789; Sigma-Aldrich); and AY9944 (2 μM; Tocris Bioscience).

RNA Extraction and PCR. Mouse brain tissues were dissected and quickly frozen at −80 °C. The total RNA from mouse brain or HeLa cells was extracted using TRIzol (Invitrogen) and purified. Complementary DNA was synthesized with SuperScript IV Reverse Transcriptase kit (Invitrogen). For RT-PCR experiments, six pairs of primers for mouse *L1CAM* mRNA were generated: pair 1, forward primer, 5′-GACTGAGCTGGCAACCTGAT-3′, and reverse primer, 5′-GAAAGAGCAGACGTGGCTTC-3′; pair 2, forward primer, 5′-GAAGCCACGTCTGCTCTTTC-3′, and reverse primer, 5′-ATGTCACCCTTGCACCTTTC-3′; pair 3, forward primer, 5′-AAGGTGCAAGGGTGACATTC-3′, and reverse primer, 5′-CTTCAAGTTCAGGGCTCACC-3′; pair 4, forward primer, 5′-AGGTGAGCCCTGAACTTGAA-3′, and reverse primer, 5′-CAGGGCCAGTTCCATTAGTC-3′; pair 5, forward primer, 5′-AGCCACAGCAGGTGAAAACT-3′, and reverse primer, 5′-CATGGCTGGACCTTGCTATT-3′; pair 6, forward primer, 5′-GAAGCTGCCCTCACTTTCTG-3′, and reverse primer, 5′-CATTTCTAGGTTTTTATTTGCCTGT-3′. For real-time PCR, mRNA expression levels in mouse brain tissues were quantitated using TaqMan probes (L1CAM, Mm00493049_m1; Actin, Mm00607939_s1; Thermo Fisher Scientific) and normalized to β-actin.

Mouse Brain MRI Analysis. Six-month-old mice were used for MRI analysis. T2-weighted MR images of the brains of *CWH43* wild-type (WT) and mutant mice were obtained, and ventricular volume was quantitated using ImageJ software (7).

Immunohistochemistry. Mice were anesthetized and perfused with 4% paraformaldehyde; the 25-μm cryostat sections of brain tissue were obtained and stored at −20 °C. Immunohistochemistry for L1CAM was performed by following several optimized steps. Briefly, cell membranes were permeabilized by incubating coverslips in PBS/0.5% Triton X-100 for 5 min. Tissue sections were then blocked in PBS containing 5% bovine serum albumin for 30–60 min at room temperature in a humidified chamber. Sections were then incubated at 4 °C overnight with primary antibody (anti-L1CAM antibody [1:500; ab24345; lot# CR324831-1, Abcam]; anti-Cwh43 antibody [1:200; Sigma; HPA048140; lot# R58111]; anti-acetylated-α tubulin [1:1,000; 5335; lot# 4; Cell Signaling Technology]; rabbit anti-plasmin antibody [OAAB11621; lot# SA100831BD; Aviva Systems Biology]). Sections were then washed in PBS and incubated in the appropriate secondary antibody (anti-mouse IgG [1:2,000; Alexa Fluor 488; A28175; Invitrogen]; goat anti-rabbit IgG [1:2,000; Alexa Fluor 546; A11035; lot #731492; Invitrogen]) for 2 h at room temperature. Tissue sections were again washed three times with PBS, and nuclei were counterstained with 4′,6-diamidino-2-phenylindole (DAPI) solution (0.2 mg/mL; Sigma-Aldrich). Confocal microscopy was performed using a Leica SP5 II confocal microscope.

Membrane and Lipid Microdomain Protein Extraction. Mouse brain tissues were dissected into ventricular and cortical regions and lysed using the Mem-PER Plus membrane protein extraction kit (Thermo Fisher Scientific) according to the manufacturer's instructions, and total membrane protein was extracted. Equal amounts of membrane protein extracts from WT and *CWH43* mutant mice were further fractionated into the aqueous and lipid compartments using Triton X-114, and the aqueous and lipid fractions were loaded in the same ratio relative to total membrane protein for Western blot analysis.

Deglycosylation Assay and Western Blot. Total protein was extracted from mouse brain tissues or cultured HeLa cells using RIPA buffer supplemented with protease inhibitors and phosphatase inhibitors. For comparisons of protein expression in the ventricular/subventricular zone and the whole brain, microdissection was performed to obtain samples from the ventricular/subventricular region. Briefly, mouse brains were sectioned coronally into 2-mm-thick sections using a commercially available mold (Zivic Instruments). The ventricular and subventricular zones at the level of the basal ganglia were then dissected (~1 mm in thickness) under the microscope using a microknife. Lysates were quantified using Pierce BCA protein assay kit (Thermo Fisher Scientific) according to the manufacturer's instructions. PNGase F (P0704S; NEB) treatment was performed according to the manufacturer's instructions. Briefly, 40 μg of protein were denatured by incubation at 100 °C for 10 min in Glycoprotein Denaturing Buffer (10×). GlycoBuffer 2 (10×), Nonidet P-40, and PNGase F were then added, followed by incubation for 1 h at 37 °C. Lysates were separated using SDS-PAGE and analyzed by Western blot. The following antibodies were used: anti–C-terminal L1CAM (OAAB11621, Aviva Systems Biology); anti–β-Actin (4970S; Cell Signaling Technology); and an anti-rabbit secondary antibody. Immunostained bands were detected using the chemiluminescent method (Pierce ECL Western Blotting Substrate; Thermo Fisher Scientific), and images were obtained using a KODAK Image Station 4000 System. Western blot quantification was performed using ImageJ software.

Three short hairpin RNAs (shRNAs) directed against plasminogen were purchased from Millipore Sigma (TRCN0000072315, TRCN0000072316, TRCN0000072317) and pooled to transfect HeLa cells. An empty control shRNA vector (pLKO.1) was used as a control. Cells were cultured in DMEM with 10% fetal bovine serum for 2 d before transfer into EX-CELL HeLa Serum-Free Medium for 48 h. The cells were then lysed in RIPA buffer supplemented with proteinase and phosphatase inhibitors. One hundred micrograms of total protein were loaded for Western blot analyses. The anti-plasminogen antibody was purchased from Boster Biological Technology (catalog #A03674-1). β-Actin was used as a loading control. The intensity of the upper band at 240 kDa relative to control cells is shown at the top of the Western blot.

Mass Spectrometry Proteomics Analysis. Cerebrospinal fluid (CSF) samples were collected stereotactically from the cisterna magna of anesthetized 3-mo-old mice. The samples were then rapidly frozen on dry ice and stored at −80 °C. WT and mutant samples were analyzed using a Thermo Scientific Q-Exactive mass spectrometer with Waters NanoAcquity UPLC at the Mass Spectrometry Facility at University of Massachusetts Medical School. The mass spectrometry proteomics data were exported and analyzed using Scaffold (Proteome Software) software.

Statistical Analysis. Throughout the different experiments, the quantification values are presented as mean ± SEM; $P > 0.05$, not significant. Differences were considered statistically significant at $P < 0.05$. Asterisks correspond to P value calculated by unpaired t test (*$P < 0.05$).

Results

iNPH-Associated CWH43 Deletion Decreases L1CAM Protein Expression in Mouse Brain. We previously reported that mice harboring iNPH-associated deletions in *CWH43* develop communicating hydrocephalus (Fig. 1*A*) (7). To determine whether alterations in L1CAM may contribute to this phenomenon, we examined L1CAM immunoreactivity in the ventricular and subventricular zone of the mouse brain using an antibody directed against the C terminus of L1CAM. In WT mice, strong L1CAM immunoreactivity was observed in neuronal somata, while less immunoreactivity was detected in the ependymal cell layer. In *CWH43* mutant mice, we observed a significant decrease in L1CAM immunoreactivity compared to WT mice (Fig. 1*B*). Real-time PCR for L1CAM mRNA obtained from the brains of these mice failed to show a significant difference (Fig. 1*C*). RT-PCR analysis using a series of overlapping primers
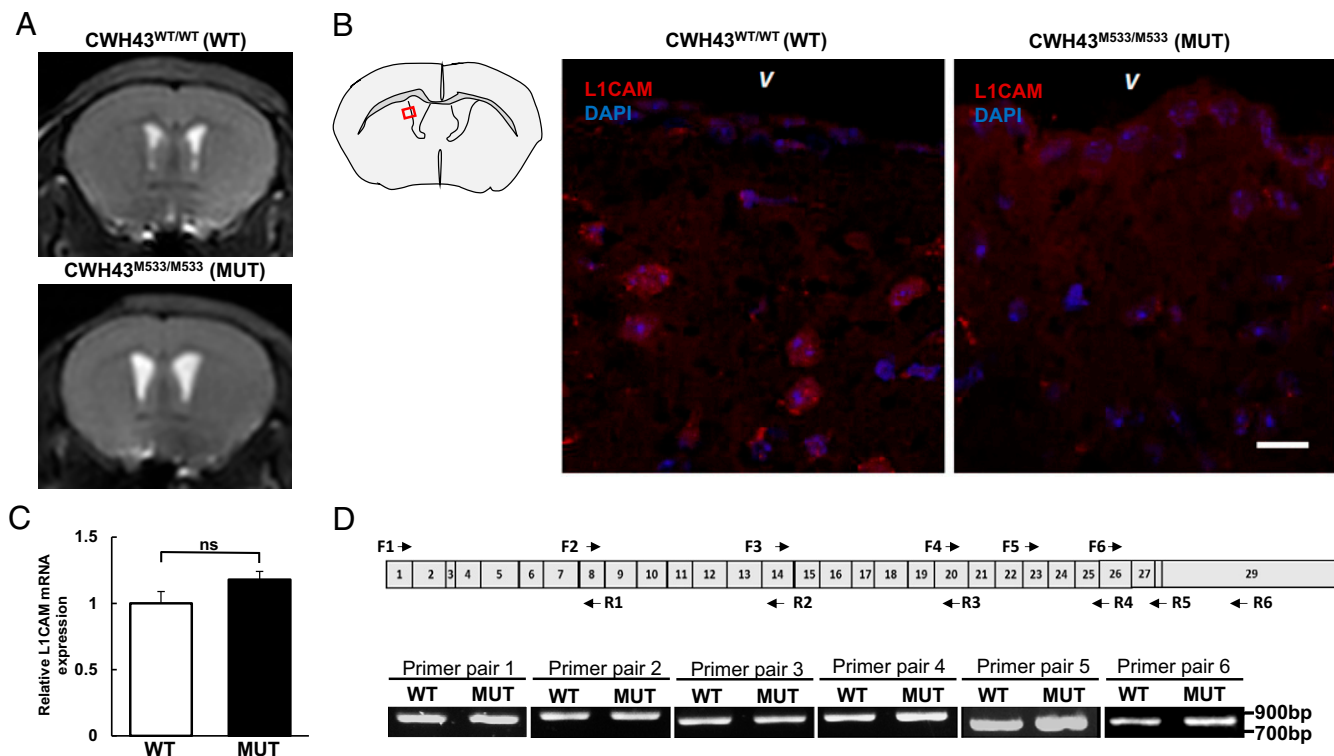
Fig. 1. *CWH43* deletion decreases L1CAM protein expression. (*A*) Representative magnetic resonance images of the brains of 6-mo-old wild-type (WT) (*Upper*) and *CWH43* homozygous mutant (MUT) (*Lower*) mice. (*B*) Confocal immunofluorescence images of the lateral ventricle area. The area within the red rectangle shown on the schematic diagram of the mouse brain (*Left*) was imaged. L1CAM immunoreactivity was visualized using anti-L1CAM antibody directed against the C terminus (red). Nuclei were counterstained with DAPI. (Scale bar: 20 μm.) (*C*) Relative L1CAM mRNA expression was measured using real-time PCR. Actin was used as a reference. Data shown are the mean ± SD from three independent experiments. Statistical significance was determined using the unpaired *t* test. (*D*) Alternative splice variant analysis of mouse brain tissue. Representative gel images showing the relative size of RT-PCR amplification products (*Lower*) and the position of the corresponding primers (*Upper*).

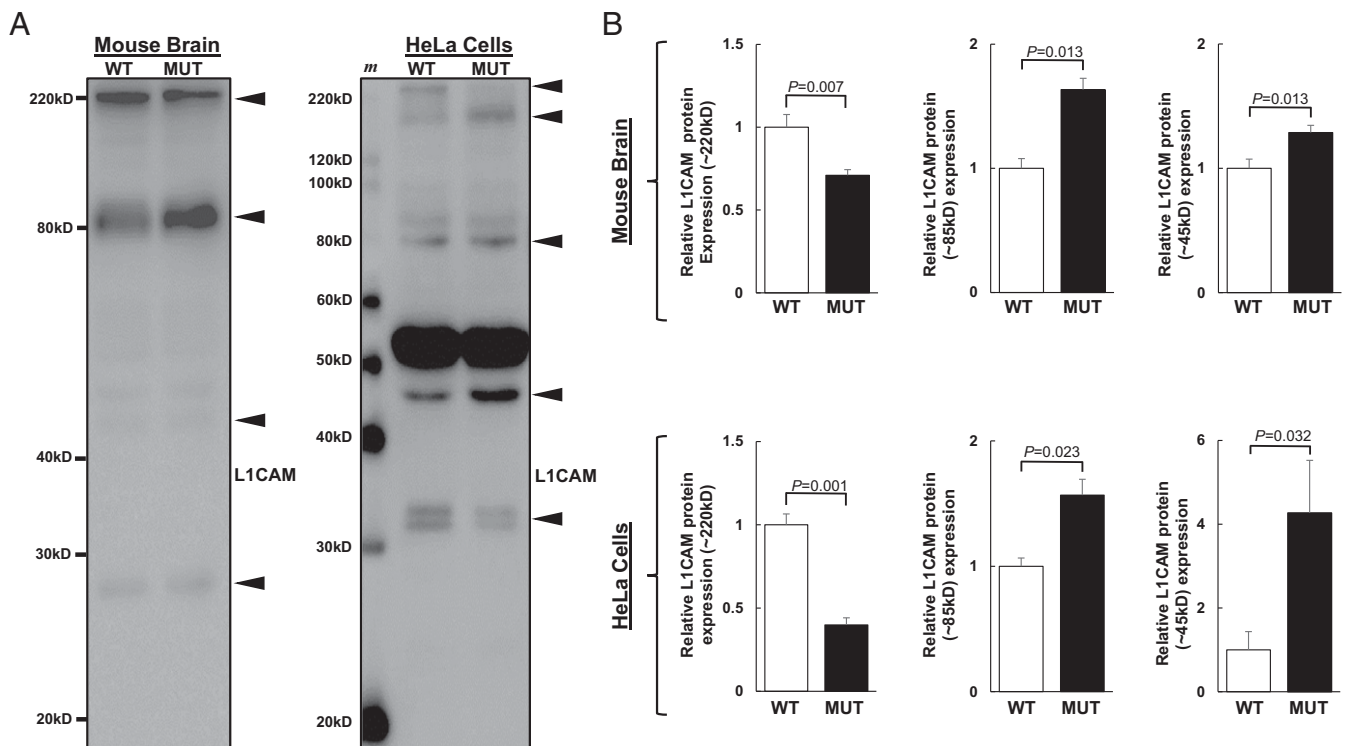indicated that there was no difference in L1CAM mRNA splicing between WT and *CWH43* mutant mice (Fig. 1*D*).

CWH43 Deletion Increases Plasmin-Mediated Proteolysis of L1CAM. To determine whether proteolysis was responsible for the decrease in full-length L1CAM expression, we used an antibody directed against the C-terminal portion of L1CAM to perform a Western blot analysis of mouse brain protein isolates (Fig. 2*A*). Because this antibody is directed against a C-terminal epitope, it recognizes the membrane-associated fragments after L1CAM cleavage but does not bind to the released soluble ectodomain fragments. A decrease in full-length L1CAM at ∼220 kDa was observed in *CWH43* mutant mice when compared to WT mice. An increase in a band at ∼85 kDa was also observed, consistent with cleavage in the FNIII3 domain by plasmin or PC5A (20, 21). Faint bands at 45 and 28 kDa were also observed.

To investigate whether the effect of *CWH43* deletion on L1CAM proteolysis was specific to the brain, we examined L1CAM expression in control human HeLa cells or in HeLa cells where a loss-of-function *CWH43* deletion had been introduced using CRISPR. As was observed in the mouse brain, a decrease in full-length L1CAM and an increase in a band at 80 kDa was detected in HeLa cells harboring the *CWH43* mutation. In HeLa cells, a clear increase in a band at ∼200 kDa was detected. Because the antibody used recognizes a C-terminal L1CAM epitope, this band likely represents differential posttranslational modification of full-length L1CAM protein and not a soluble L1CAM fragment. A band at ∼45 kDa was also noted to increase in *CWH43* mutant HeLa cells. The identity of the protease(s) responsible for producing this fragment is unclear. Importantly, a decrease in

a 32-kDa band representing a C-terminal L1CAM fragment was observed (Fig. 2*A*). This fragment has been reported to be generated when full-length L1CAM is proximally cleaved by ADAM10 or BACE1 (18, 19). Quantification of changes in each of these bands is shown in Fig. 2*B*. Human and mouse L1CAM are 92% identical. There are two main isoforms in humans, and at least three in mice. Each of these can be posttranslationally modified and cleaved by a number of different enzymes and proteases in a tissue-specific manner. This may explain differences in the apparent molecular weight of L1CAM bands seen on gel electrophoresis studies using protein derived from mouse brain and human HeLa cells. Taken together, these data revealed alterations in the proteolytic cleavage of L1CAM in the context of *CWH43* mutation in the mouse brain in vivo and in human HeLa cells in vitro.

The changes in L1CAM proteolysis seen on Western blot suggested an overall increase in L1CAM cleavage, with a relative increase in cleavage in the FNIII3 domain (85-kDa fragment) and decreased cleavage proximally near the transmembrane domain (32-kDa fragment). Plasmin cleaves L1CAM at sites located in the FNIII3 domain, generating an 80- to 85-kDa membrane-associated fragment (20). We confirmed that the addition of plasmin to WT HeLa cells maintained in a serum-free medium decreased the expression of full-length L1CAM (220 kDa) and increased the abundance of the 80- to 85-kDa fragment in a concentration-dependent manner. Interestingly, the fragment at ∼200 kDa was unchanged in WT HeLa cells after plasmin exposure (Fig. 3*A*). However, in HeLa cells harboring a homozygous deletion of *CWH43*, exposure to plasmin decreased the 220-, 200-, and 85-kDa bands. This response to plasmin has previously been

Yang et al.
Increased plasmin-mediated proteolysis of L1CAM in a mouse model of idiopathic normal pressure hydrocephalus

PNAS | 3 of 8
https://doi.org/10.1073/pnas.2010528118
www.manaraa.com

Fig. 2. *CWH43* deletion increases L1CAM proteolysis. (*A*) Western blot analysis for L1CAM in protein extracts obtained from mouse brain (WT and *CWH43* homozygote, *Left*) and HeLa cells (WT and *CWH43* homozygote, *Right*). (*B*) Quantification of data from Western blot analyses of L1CAM protein levels. Data shown are mean ± SEM from three independent experiments (*n* = 3). β-Actin was used as a loading control. Statistical significance was determined using the unpaired *t* test.

reported and is indicative of extended L1CAM proteolysis at higher levels of plasmin activity (20).

The plasmin inhibitor, α2 antiplasmin (22), failed to increase the band at 220 kDa or decrease the band at 80–85 kDa in WT HeLa cells, suggesting that plasmin does not play a significant role in L1CAM proteolysis at baseline in these cells. In contrast, α2 antiplasmin increased the 220-kDa band and decreased the 80- to 85-kDa band in *CWH43* mutant HeLa cells. Taken together, these data suggest that loss of *CWH43* function increases L1CAM sensitivity to plasmin proteolysis.

Constitutive shedding of L1CAM is mediated by ADAM10 in many cell types (19). Exposure of WT HeLa cells to the ADAM10 inhibitor, GI254023X, led to a slight increase in the expression of full-length L1CAM at 220 kDa, indicating a low level of constitutive ADAM10 proteolysis of L1CAM (Fig. 3*C*). GI254023X also led to a slight increase in full-length L1CAM in *CWH43* mutant HeLa cells, indicating a small contribution to L1CAM proteolysis by ADAM10 in these cells as well. Interestingly, ADAM10 inhibition preferentially increased the abundance of the 45-kDa L1CAM fragment in *CWH43* mutant but not WT HeLa cells, suggesting that this fragment may undergo proteolysis by ADAM10 specifically in the context of *CWH43* deletion.

Cleavage of L1CAM by plasmin generates a 140-kDa ectodomain fragment that is soluble and can be deposited in the extracellular matrix (20). We therefore used mass spectrometry to look for shedding of L1CAM in CSF obtained from the mouse brain. Soluble L1CAM was not detected in the CSF of adult WT mice (*n* = 6), but it was detected in each of the CSF samples obtained from *CWH43* mutant mice (*n* = 6; Fig. 3*D*). Analysis of the peptide sequences indicated that all of the peptides identified were from the L1CAM ectodomain distal to the plasmin cleavage site (Fig. 3*E*), consistent with plasmin proteolysis.

CWH43 Deletion Results in L1CAM Hypoglycosylation and Reduced Lipid Microdomain Localization. Our findings suggested that the increased L1CAM proteolysis observed in *CWH43* mutant cells was due to increased sensitivity of L1CAM to plasmin cleavage. Western blot analysis of HeLa cell protein isolates consistently showed an increased band at 200 kDa (Fig. 4*A*). This band has been reported to represent a hypoglycosylated form of full-length L1CAM (13). Exposure of HeLa cell protein isolates to peptide: N-glycosidase F (PNGase F), an enzyme that removes almost all N-linked oligosaccharides from glycoproteins, confirmed that this band corresponded to hypoglycosylated full-length L1CAM (Fig. 4*B*).

L1CAM has been associated with cholesterol-rich microdomains in the cell membrane that have been referred to as lipid rafts (23). Studies indicate that glycosylation can promote trafficking of proteins to lipid microdomains (24, 25). We therefore used Triton X-114 extraction to examine the association of L1CAM with lipid microdomains in protein isolates from WT or *CWH43* mutant mouse brain. Decreased L1CAM was identified in the lipid fraction in *CWH43* mutant mice when compared to WT mice (Fig. 4*C*). Disruption of these cholesterol-rich lipid microdomains using an inhibitor of cholesterol biosynthesis, AY-9944, decreased the amount of L1CAM protein expressed in HeLa cells (Fig. 4*D*). Previous studies have reported that cholesterol depletion leads to the cleavage of L1CAM in released microvesicles containing both L1CAM and ADAM10 (26).

Our data indicated that decreased glycosylation of L1CAM in CWH43 mutant cells makes it more sensitive to proteolytic cleavage, and our studies using exogenous plasmin or alpha 2 antiplasmin thus implicated plasmin as the protease responsible for this cleavage. To further determine whether plasmin is responsible for the observed effects on L1CAM, we used an shRNA directed against plasminogen to knock down plasmin expression in HeLa
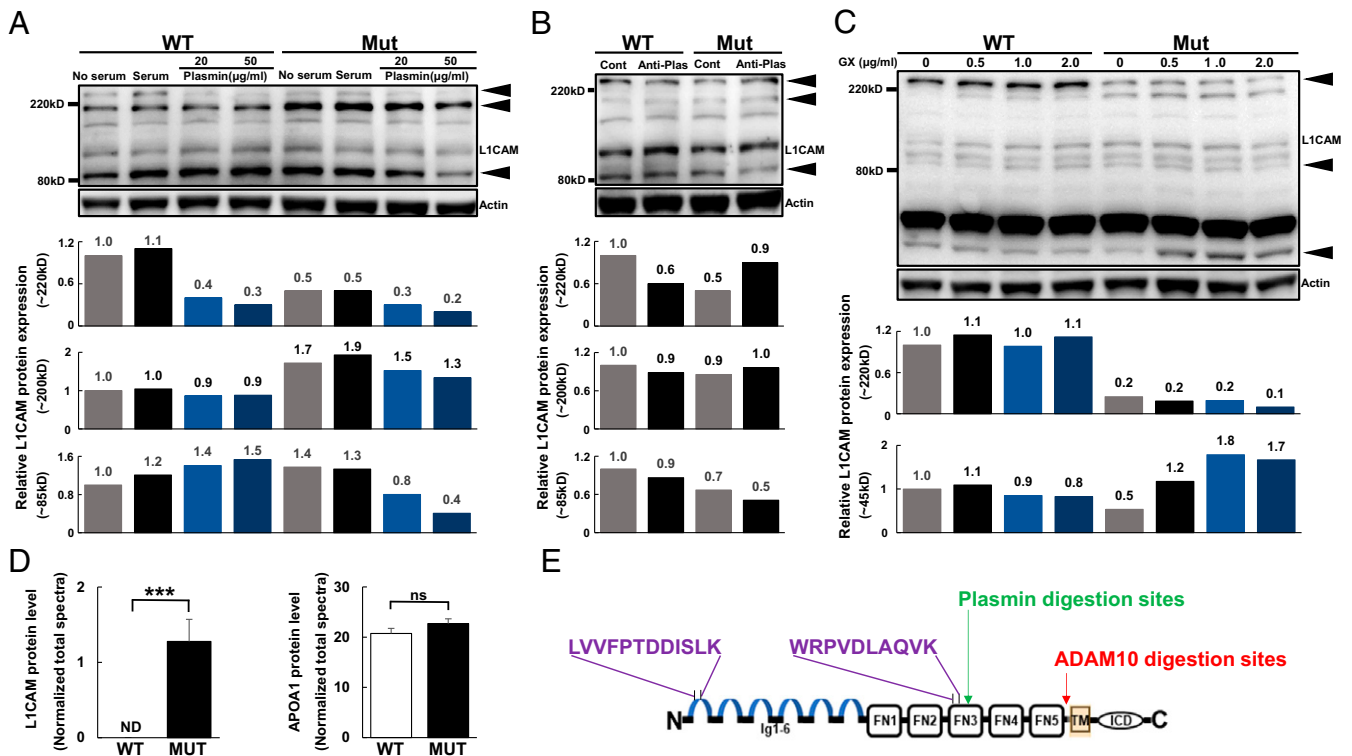
Fig. 3. Plasmin mediates increased L1CAM proteolysis after *CWH43* deletion. (*A*) Western blot analysis of L1CAM protein expression in HeLa cells. WT and *CWH43* mutant HeLa cells were maintained in serum-free medium, medium containing 10% serum, or serum-free medium supplemented with recombinant human plasmin (20 or 50 μg/m). Bar graphs below each blot quantitate changes in band intensities on each blot. β-Actin was used as a loading control. (*B*) WT or *CWH43* mutant HeLa cells were treated with 70 μg/mL α2 antiplasmin. (*C*) WT or *CWH43* mutant HeLa cells were incubated in the presence of the ADAM10 inhibitor, GI254023X, at the indicated concentrations. (*D*) Mass spectrometry analysis of mouse brain CSF. Relative L1CAM peptide levels were quantified based on the normalized total spectra (*Left*). APOA1 protein is presented as a control (*Right*). The data shown were obtained from two pairs of WT and *CWH43* mutant mice with three replicates for each sample and represent the mean ± SEM. Statistical significance was determined using the unpaired *t* test. ***P = 0.0036. (*E*) Schematic diagram showing the L1CAM peptides detected in CSF from CWH43 mutant mice. Known plasmin digestion sites (green arrow) and ADAM10 digestion sites (red arrow) are as shown.

cells maintained in a serum-free medium. As shown in Fig. 4*E*, plasmin knockdown in *CWH43* mutant HeLa cells increased the amount of full-length L1CAM and decreased the amount of L1CAM cleavage (as indicated by a decrease in the 80- and 45-kDa bands).

CWH43 Deletion Reduces the Level of L1CAM Intracellular Fragment in CWH43-Expressing Cells. Cleavage of L1CAM by ADAM10 or BACE 1 generates a 32-kDa membrane-associated intracellular fragment that is further cleaved by γ-secretase to yield a 28-kDa intracellular fragment representing the L1CAM intracellular domain (ICD) (19). The L1CAM ICD can then translocate to the nucleus to regulate transcription. Generation of the 32- and 28-kDa C-terminal intracellular fragments is thus important for L1CAM nuclear signaling. Western blot analysis of HeLa cell protein lysates revealed decreased expression of the 32-kDa membrane-associated intracellular fragment in *CWH43* mutant cells when compared to WT cells (Fig. 5*A*). The 28-kDa intracellular fragment was not detected in these cells.
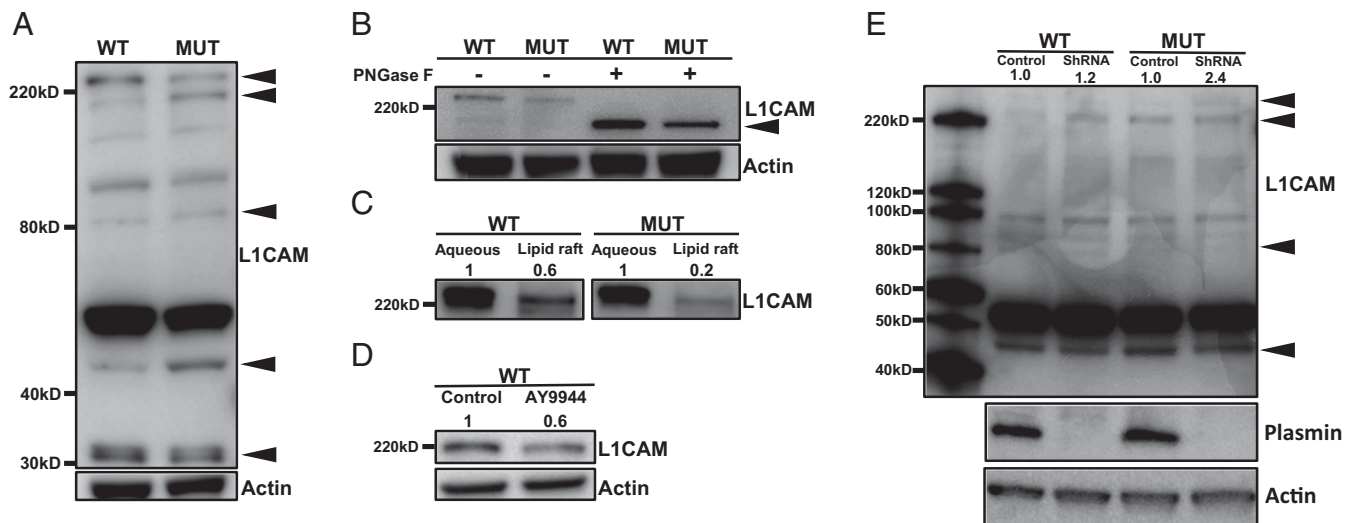
In the adult mouse brain (6 mo), *CWH43* mRNA and protein expression are expressed primarily in the ventricular/subventricular zone and in a small set of neuronal subpopulations (Fig. 5*B*). This distribution of Cwh43 expression suggests that the effect of *CWH43* deletion on L1CAM proteolysis should be manifest primarily in those areas. Western blot analysis of lysates obtained from the mouse ventricular/subventricular zone and from the cortex indicated that decreases in full-length L1CAM and in the 28-kDa intracellular fragment were present in the ventricular zone but

not in the cortex (Fig. 5*C*). Immunohistochemistry using an antibody directed against the C terminus of L1CAM showed decreased nuclear L1CAM immunoreactivity in *CWH43* mutant mice when compared to WT mice. Taken together, these data reveal increased plasmin-mediated L1CAM proteolysis and decreased L1CAM nuclear translocation in the ventricular/subventricular zone of the mouse brain and in cultured human cells harboring *CWH43* deletions.

Discussion

The hydrocephalus, gait dysfunction, incontinence, and dementia that characterize iNPH usually appear after the age of 60, with most iNPH patients being asymptomatic and behaviorally normal prior to disease onset (1, 2). We recently reported that loss-of-function deletions in *CWH43* are enriched among patients with sporadic iNPH and cause an iNPH-like syndrome in genetically engineered mice (7). *CWH43* mutant mice develop communicating hydrocephalus and thus provide a useful tool for studying the mechanisms underlying iNPH. Here, we show that *CWH43* deletion leads to hypoglycosylation of L1CAM, decreased association of L1CAM with lipid microdomains in the cell membrane, increased cleavage of L1CAM by plasmin, decreased L1CAM nuclear translocation, and decreased L1CAM expression in the ventricular/subventricular zone.

Loss-of-function mutations in *L1CAM* cause congenital hydrocephalus and a range of severe neurodevelopmental abnormalities (9). When introduced into mice, *L1CAM* mutations cause congenital hydrocephalus and neurodevelopmental abnormalities

Yang et al.
Increased plasmin-mediated proteolysis of L1CAM in a mouse model of idiopathic normal pressure hydrocephalus

PNAS | 5 of 8
https://doi.org/10.1073/pnas.2010528118
www.manaraa.com

Fig. 4. *CWH43* deletion decreases L1CAM glycosylation and association with lipid microdomains. (*A*) Western blot analysis of L1CAM protein expression in HeLa cells. The arrowheads point to bands representing L1CAM protein fragments of interest in WT and *CWH43* mutant HeLa cells. β-Actin was used as a loading control. (*B*) Protein extracts from WT and CWH43 mutant cells were incubated with the deglycosylating enzyme PNGase F and compared to control protein extracts using Western blot. Representative images showing differential amounts of glycosylated (upper band) and deglycosylated (lower band) full-length L1CAM at ∼220 kDa in WT and *CWH43* mutant HeLa cells. β-Actin was used as a loading control. (*C*) Western blot analysis of aqueous- and lipid-phase extracts derived from equivalent amounts of total membrane protein obtained from WT and *CWH43* mutant mouse brain. The ratios of band intensities for L1CAM protein in the aqueous and the lipid phases were quantified and are shown at the top of the blot. (*D*) WT HeLa cells were cultured in control medium or medium supplemented with the cholesterol synthesis inhibitor AY9944 (2 μM). The intensity of each band was quantified using ImageJ and the ratio relative to actin loading control was calculated. β-Actin was used as a loading control. (*E*) WT and *CWH43* mutant HeLa cells were transfected with a control shRNA or a pool of three shRNAs directed against plasminogen. The cells were then transferred to a serum-free medium. After 48 h, protein was collected for Western blot analysis of L1CAM expression. Plasmin knockdown was confirmed using a specific anti-plasmin antibody. β-Actin was used as a loading control. The intensity of the upper band at 240 kDa relative to control cells is shown at the top of the Western blot.

similar to those observed in humans (11). Many disease-causing mutations in *L1CAM* decrease cell surface expression of the protein or otherwise disrupt L1CAM homophilic or heterophilic binding to other proteins (27).

Unlike the congenital hydrocephalus and developmental abnormalities that are frequently seen with *L1CAM* mutations, iNPH manifests late in life in previously asymptomatic individuals (2–6). Hydrocephalus and gait abnormalities are detectable in *CWH43* mutant mice during early adulthood. However, these mice do not display gross anatomic abnormalities of brain development or severe behavioral deficits despite the finding that L1CAM expression is decreased. Our data provide several possible explanations for this observation. First, *CWH43* deletion down-regulates (but does not eliminate) expression of full-length L1CAM. Second, studies in zebrafish suggest that the cleaved L1CAM ectodomain corresponding to the ADAM10 cleavage product can partially (although not completely) rescue the hydrocephalus phenotype in zebrafish lacking endogenous full-length L1CAM (18). Third, we found that the down-regulation of L1CAM expression is localized primarily to the ventricular and subventricular zones where Cwh43 is most highly expressed. The net result is decreased expression of L1CAM primarily in the ventricular/subventricular zone where Cwh43 is most highly expressed.

The increased proteolysis of L1CAM observed in the current study appears to be due to increased sensitivity of the protein to plasmin cleavage in cells harboring *CWH43* deletions. One contributor to this increased sensitivity may be hypoglycosylation of L1CAM, as was observed in HeLa cells harboring *CWH43* deletion. Under normal conditions, L1CAM is heavily glycosylated, and this glycosylation regulates its interactions with other proteins (13). Three glycosylation sites are located near the plasmin cleavage sites in the FNIII3 domain. Core fucosylation at these sites precludes plasmin cleavage of L1CAM in melanoma cells (15). Our data suggest that hypoglycosylation exposes

these sites, thereby increasing the sensitivity of L1CAM to plasmin cleavage, as has been demonstrated in melanoma cells.

Previous studies have indicated that hypoglycosylation decreases L1CAM cell surface expression and heterophilic binding (13). Interestingly, L1CAM activation regulates cell surface glycosylation by increasing the expression of ST6Gal1 (β-galactoside α-2,6-sialyltransferase) and FUT9 (fucosyltransferase). Inhibitors of sialylation and fucosylation block L1CAM-induced cell migration and survival in Chinese hamster ovary cells while decreasing FUT9 and ST6Gal1 expression via PI3K- and Erk-dependent signaling pathways (28). Thus, additional studies are needed to determine whether the hypoglycosylation and decreased expression of L1CAM observed after *CWH43* deletion are accompanied by more widespread defects in protein glycosylation.

Lipid microdomains are thought to act as platforms where proteins cluster together to interact and participate in cell signaling functions. Previous studies have shown that L1CAM associates with lipid microdomains where it interacts with other proteins such as growth factor receptors or CD24 (29, 30). Alcohol increases the trafficking of L1 into lipid microdomains and inhibits L1CAM-induced neurite outgrowth, although subsequent studies have suggested that alcohol inhibition of L1CAM-induced neurite outgrowth does not require recruitment of the protein into lipid microdomains (23). Disruption of lipid rafts by cholesterol depletion induces the release of microvesicles in which L1CAM is cleaved by ADAM10, demonstrating that L1CAM proteolysis by ADAM10 can occur both inside and outside lipid microdomains (26). We observed that *CWH43* deletion decreases the association of L1CAM with cholesterol-rich lipid microdomains on the cell membrane and increases plasmin cleavage of L1CAM. Given the concomitant decrease in glycosylation, it will be important to determine whether L1CAM interactions with other proteins are altered in cells harboring *CWH43* deletions.
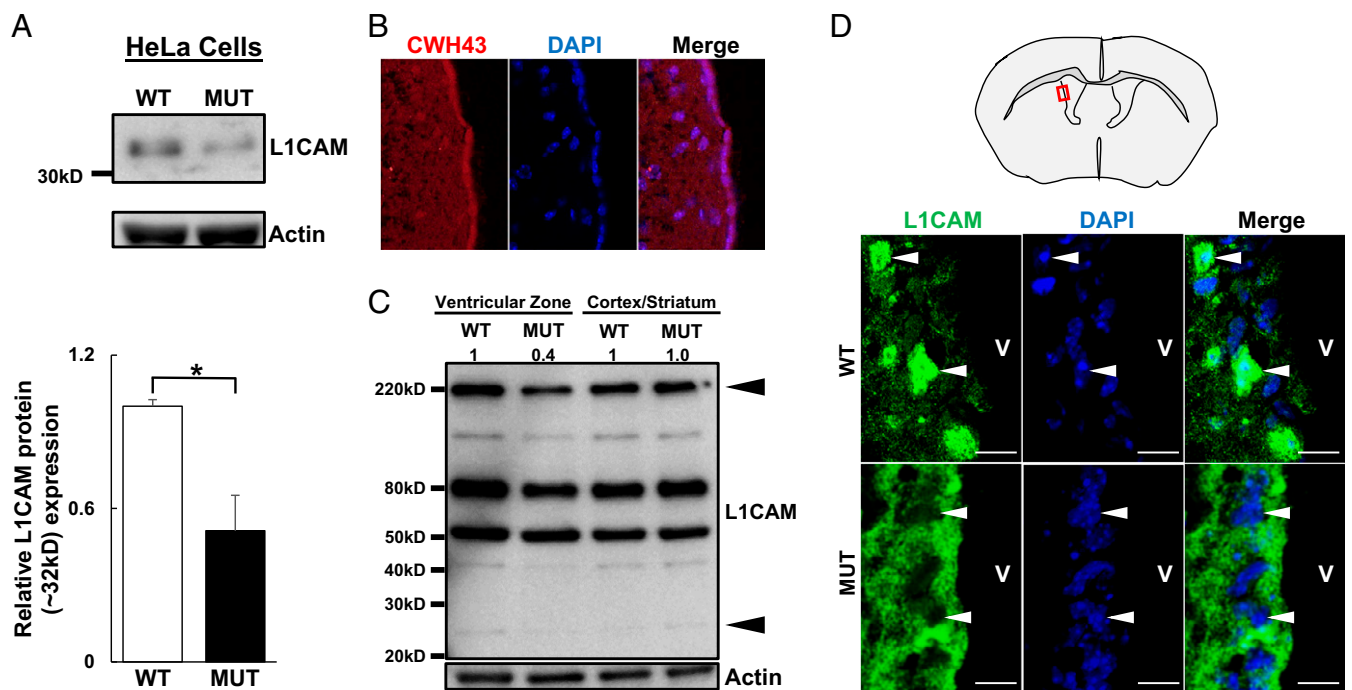
Fig. 5. *CWH43* deletion decreases *L1CAM* nuclear localization. (*A*) Western blot analysis showing abundance of the ~32-kDa L1CAM intracellular fragment. β-Actin was used as loading control. Data were obtained from three independent experiments and represent the mean ± SEM. Statistical significance was calculated using the unpaired *t* test, *$P = 0.029$. (*B*) Immunofluorescence micrographs showing localization of Cwh43 immunoreactivity (red) in the ventricular region of the mouse brain. Cilia are stained using an antibody directed against acetylated α-tubulin (green). Nuclei are counterstained with DAPI. The ventricle (V) is identified. (Scale bar: 25 μm.) (*C*) Western blot analysis of L1CAM protein levels in the ventricular zone and cortex/striatum of WT and *CWH43* mutant mouse brain. An antibody directed against the C terminus of L1CAM was used. Arrowheads identify L1CAM bands of interest. (*D*) Immunofluorescence micrographs showing the distribution of L1CAM immunoreactivity (green) in the ventricular zone of WT and *CWH43* mutant mice. An antibody directed against the C terminus of L1CAM was used. Nuclei are counterstained with DAPI (blue). Note the presence of nuclear L1CAM immunoreactivity in the WT but not the *CWH43* mutant cells. (Scale bar: 25 μm.)

Although it is clear that disruption of L1CAM function causes hydrocephalus, the exact mechanism by which this occurs remains poorly understood. Overexpression of the soluble L1CAM ectodomain generated by ADAM10 cleavage, or overexpression of an ADAM10-resistant form of L1CAM was as effective as overexpression of the full-length WT L1CAM in rescuing the hydrocephalus phenotype observed in *L1CAM* mutant zebrafish (18). Importantly, only a partial rescue of the hydrocephalus phenotype could be achieved by overexpressing any one of these L1CAM forms in the zebrafish model. Our findings suggest that hydrocephalus due to decreased L1CAM expression can occur in the absence of major neurodevelopmental defects if the decrease in expression is incomplete and anatomically restricted. The fact that the decrease in L1CAM expression occurs primarily in the ventricular and subventricular zone in *CWH43* mutant mice

suggests that L1CAM may regulate ventricular size through local interactions in the periventricular region. L1CAM hypoglycosylation, decreased localization to lipid microdomains, and decreased expression are all predicted to reduce L1CAM homophilic and heterophilic binding. Our data suggest that L1CAM nuclear signaling may be decreased as well. Future studies will examine how the observed changes in L1CAM alter ventricular size.

1. R. D. Adams, C. M. Fisher, S. Hakim, R. G. Ojemann, W. H. Sweet, Symptomatic occult hydrocephalus with "normal" cerebrospinal-fluid pressure. A treatable syndrome. *N. Engl. J. Med.* **273**, 117–126 (1965).
2. T. T. Hickman *et al.*, Association between shunt-responsive idiopathic normal pressure hydrocephalus and alcohol. *J. Neurosurg.* **127**, 240–248 (2017).
3. N. Tanaka, S. Yamaguchi, H. Ishikawa, H. Ishii, K. Meguro, Prevalence of possible idiopathic normal-pressure hydrocephalus in Japan: The Osaki-Tajiri Project. *Neuroepidemiology* **32**, 171–175 (2009).
4. K. Hiraoka, K. Meguro, E. Mori, Prevalence of idiopathic normal-pressure hydrocephalus in the elderly population of a Japanese rural community. *Neurol. Med. Chir. (Tokyo)* **48**, 197–200 (2008).
5. R. Martín-Láez, H. Caballero-Arzapalo, L. A. López-Menéndez, J. C. Arango-Lasprilla, A. Vázquez-Barquero, Epidemiology of idiopathic normal pressure hydrocephalus: A systematic review of the literature. *World Neurosurg.* **84**, 2002–2009 (2015).
6. D. Jaraj *et al.*, Prevalence of idiopathic normal-pressure hydrocephalus. *Neurology* **82**, 1449–1454 (2014).
7. H. W. Yang *et al.*, Deletions in CWH43 cause idiopathic normal pressure hydrocephalus. *EMBO Mol. Med.* **13**, e13249 (2021).

8. V. Ghugtyal, C. Vionnet, C. Roubaty, A. Conzelmann, CWH43 is required for the introduction of ceramides into GPI anchors in *Saccharomyces cerevisiae. Mol. Microbiol.* **65**, 1493–1502 (2007).
9. H. Adle-Biassette *et al.*, Neuropathological review of 138 cases genetically tested for X-linked hydrocephalus: Evidence for closely related clinical entities of unknown molecular bases. *Acta Neuropathol.* **126**, 427–442 (2013).
10. M. V. Maten, C. Reijnen, J. M. A. Pijnenborg, M. M. Zegers, L1 cell adhesion molecule in cancer: A systematic review on domain-specific functions. *Int. J. Mol. Sci.* **20**, 4180 (2019).
11. H. Kamiguchi, M. L. Hlavin, V. Lemmon, Role of L1 in neural development: What the knockouts tell us. *Mol. Cell. Neurosci.* **12**, 48–55 (1998).
12. P. F. Maness, M. Schachner, Neural recognition molecules of the immunoglobulin superfamily: Signaling transducers of axon guidance and neuronal migration. *Nat. Neurosci.* **10**, 19–26 (2007).
13. D. Medina-Cano *et al.*, High N-glycan multiplicity is critical for neuronal adhesion and sensitizes the developing cerebellum to N-glycosylation defect. *eLife* **7**, e38309 (2018).
14. M. Gschwandtner *et al.*, Proteome analysis identifies L1CAM/CD171 and DPP4/CD26 as novel markers of human skin mast cells. *Allergy* **72**, 85–97 (2017).

Yang et al.
Increased plasmin-mediated proteolysis of L1CAM in a mouse model of idiopathic normal pressure hydrocephalus

PNAS | 7 of 8
https://doi.org/10.1073/pnas.2010528118

15. P. Agrawal *et al*., A systems biology approach identifies FUT8 as a driver of melanoma metastasis. *Cancer Cell* **31**, 804–819.e7 (2017).

16. D. Lutz *et al*., Myelin basic protein cleaves cell adhesion molecule L1 and promotes neuritogenesis and cell survival. *J. Biol. Chem.* **289**, 13503–13518 (2014).

17. D. Lutz *et al*., Proteolytic cleavage of transmembrane cell adhesion molecule L1 by extracellular matrix molecule Reelin is important for mouse brain development. *Sci. Rep.* **7**, 1–15 (2017).

18. C. Linneberg, C. L. F. Toft, K. Kjaer-Sorensen, L. S. Laursen, L1cam-mediated developmental processes of the nervous system are differentially regulated by proteolytic processing. *Sci. Rep.* **9**, 1–14 (2019).

19. T. Maretzky *et al*., L1 is sequentially processed by two differently activated metalloproteases and presenilin/gamma-secretase and regulates neural cell adhesion, cell migration, and neurite outgrowth. *Mol. Cell. Biol.* **25**, 9040–9053 (2005).

20. N. Nayeem *et al*., A potential role for the plasmin(ogen) system in the posttranslational cleavage of the neural cell adhesion molecule L1. *J. Cell Sci.* **112**, 4739–4749 (1999).

21. I. Kalus, B. Schnegelsberg, N. G. Seidah, R. Kleene, M. Schachner, The proprotein convertase PC5A and a metalloprotease are involved in the proteolytic processing of the neural adhesion molecule L1. *J. Biol. Chem.* **278**, 10381–10388 (2003).

22. S. L. Carpenter, P. Mathew, Alpha2-antiplasmin and its deficiency: Fibrinolysis out of balance. *Haemophilia* **14**, 1250–1254 (2008).

23. X. Dou, M. E. Charness, Effect of lipid raft disruption on ethanol inhibition of L1 adhesion. *Alcohol. Clin. Exp. Res.* **38**, 2707–2711 (2014).

24. G. Chen *et al*., Mature N-linked glycans facilitate UT-A1 urea transporter lipid raft compartmentalization. *FASEB J.* **25**, 4531–4539 (2011).

25. B. Shao *et al*., O-glycans direct selectin ligands to lipid rafts on leukocytes. *Proc. Natl. Acad. Sci. U.S.A.* **112**, 8661–8666 (2015).

26. P. Gutwein *et al*., ADAM10-mediated cleavage of L1 adhesion molecule at the cell surface and in released membrane vesicles. *FASEB J.* **17**, 292–294 (2003).

27. H. D. Moulding, R. L. Martuza, S. D. Rabkin, Clinical mutations in the L1 neural cell adhesion molecule affect cell-surface expression. *J. Neurosci.* **20**, 5696–5702 (2000).

28. G. Shi *et al*., Cell recognition molecule L1 regulates cell surface glycosylation to modulate cell survival and migration. *Int. J. Med. Sci.* **14**, 1276–1283 (2017).

29. H. Joseph, *et al*, Structural determinants and functional consequences of protein affinity for membrane rafts. *Nat. Commun.* **8**, 1–10 (2017).

30. D. C. Ayre, S. L. Christian, CD24: A rheostat that modulates cell surface receptor signaling of diverse receptors. *Front. Cell Dev. Biol.* **4**, 146 (2016).